Spatiotemporal Correlation Analysis of Cardiac Activation Patterns In Langendorff-Perfused Human Hearts: Insights For Arrhythmia Prediction

Anna Crispino[1], Alessandro Loppini[1], Ilija Uzelac[2], Simonetta Filippi[1], Flavio H. Fenton[2], Alessio Gizzi[1]

[1]University Campus Bio-Medico of Rome, Rome, Italy
[2]Georgia Institute of Technology, Atlanta, USA

Abstract

Electric instabilities in cardiac dynamics, arising in the form of action potential duration alternans in time and space, are well-established precursors of arrhythmias and ventricular fibrillation leading to sudden cardiac death. Mechanisms associated with the appearance of these instabilities were pointed out to be linked both to cellular-level features and to the dynamic response of cardiac tissues resulting from heterogeneity and anisotropy. In this framework, transmural dispersion has been shown to play a fundamental role in shaping the evolution of alternans patterns and in the degeneration of cardiac rhythms into fibrillation. This contribution presents a case of study of human heart endocardium and epicardium surfaces during pacing-down restitution protocols recorded through optical mapping. We quantify alternans onset and development on both surfaces, further investigating differences in conduction velocity and correlation properties. Our results show a significant dispersion between endocardium and epicardium, corroborating the prominent role of such a biomarker in predicting arrhythmias and fibrillation.

1. Introduction

Maintaining a normal cardiac rhythm requires an organized depolarization, propagation, and repolarization of the cardiac action potential at both the cellular and tissue levels [1,2]. T-wave alternans (TWA) is an important biomarker used to predict arrhythmias and sudden cardiac death, and disruptions in action potential generation at these levels have been linked to its genesis [3]. At the cellular level, pro-arrhythmic conditions result in beat-to-beat alternation in both intracellular calcium and action potential duration (APD) under fast-pacing regimes [4,5]. At the tissue level, alternans can be defined as spatially concordant (SCA), when the entire tissue exhibits in-phase alternans, or discordant (SDA) characterized by out-of-phase alternans in multiple tissue regions separated by nodal lines [6, 7]. SDA's intrinsic characteristics and related complex alternans patterns are of great interest as they can potentially produce large spatial dispersion of repolarization, thus inducing conduction block and reentry. Moreover, transmural dispersion of repolarization has been shown to play a role in the genesis of ventricular tachycardia and fibrillation [8].

To comprehensively analyze cardiac activation patterns, it is necessary to compare the dynamics of epicardium and endocardium surfaces [9]. Several studies have shown that the electrical activity of the heart behaves differently through the epicardium and endocardium due to cellular heterogeneity and ion channel expression [10]. Differences in the spatiotemporal dynamics of electrical excitation can have important implications for cardiac function, arrhythmias onset and cardiac pathologies, in general.

This study proposes an experimental investigation of cardiac activation maps based on optical mapping voltage recordings on ex-vivo Langendorff-perfused human heart ventricles at physiological temperature (37°C) under pacing-down restitution protocols. We studied signal morphology, conduction velocity restitutions and alternans maps with high spatial and temporal resolutions. The analysis is further enriched with a spatiotemporal correlation analysis to extract the characteristic spatial length (L_0) [cm] from simultaneous endocardium and epicardium recordings.

Overall, we propose a case of study of a single human ventricular epicardium and endocardium providing novel insights into predictive arrhythmic indices.

2. Materials and Methods

Ex-vivo epicardial and endocardial surfaces of one pathological human heart (affected by cardiomyopathy) were analyzed using optical mapping technique [11]. All the experiments were undertaken in accordance with ethical guidelines set out by National Institutes of Health and approved by the Office of Research and Integrity Assurance at Georgia Tech.

2.1. Experimental framework

A Langendorff-perfused human heart ventricle under the full pacing-down restitution protocol [9] is considered. The protocol involves gradually reducing the pacing rate (PCL) of current stimulus applied on the tissue surface, starting from 1000 ms down to fibrillation or conduction block onset. Tissue preparation and stimulation protocol

were described in detail in [6]. Data were collected with an acquisition frequency of 500 Hz simultaneously for voltage and intracellular calcium, and with a spatial resolution of 0.065-0.05 cm/pixel for epi-endocardial tissues.

2.2. Data processing

Optical signals were analyzed through a semi-automatic custom MATLAB algorithm that performs on fluorescence signals (i) a removal of drift and (ii) reduction of fluorescence-induced noise using a spatial Gaussian filter (window = 7 and standard deviation = 2) combined with temporal filtering for each time series, i.e., Savitzky-Golay filter (window size = 21, polynomial order = 5). This method allows for noise reduction while maintaining the original signal shape [12]. Finally, a pixel-to-pixel normalization was carried out, and a binary mask was evaluated by excluding pixels with a signal-to-noise ratio (SNR) lower than 10 dB.

2.3. Alternans measure

Spatio-temporal analysis of voltage alternans is conduced computing APD_{75} index (Fig.1) associated with a thresholding mechanism (thr = 5 ms):

$$\begin{aligned} \Delta\mathrm{APD}_n(x,y) &= \mathrm{APD}_{n+1}(x,y) - \mathrm{APD}_n(x,y) \\ |\Delta\mathrm{APD}(x,y)| \geq thr &\quad alternans \\ |\Delta\mathrm{APD}(x,y)| < thr &\quad nodal\ lines \end{aligned} \tag{1}$$

where $\mathrm{APD}_n(x,y)$ is the action potential duration related to a specific pixel inside a 2D-field (Fig.1) measured with 75% of repolarization threshold. Each dataset was then averaged over time and space to build a global restitution curve for long and short beats (not shown). According to Eq.1, spatial alternans maps are shown with red-green-white color scale.

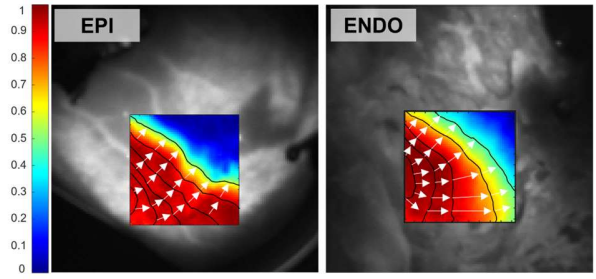

Figure 1. Schematic diagram showing the 2D-fields (51x51 pixels) for epicardium (EPI) and endocardium (ENDO) with isochrones (black lines) calculated at 50% of depolarization together with representative normal direction to the wavefront propagation (white lines).

2.4. Conduction velocity

A custom MATLAB algorithm was used for conduction velocity (CV) calculation in cardiac tissue, which identifies at first wavefront isochrones at 50% of depolarization for consecutive time steps (Fig.1). For each pair of consecutive isochrones, the algorithm selects pairs of pixels with a distance parallel to the direction normal to the wavefront and evaluates local velocities for every pair of pixels and every pair of consecutive isochrones over four beats. The mean CV values for both endocardium and epicardium were calculated for a representative tissue area of 51x51 pixels (Fig.1).

2.5. Characteristic spatial length measures

A quantitative examination of fluorescence optical mapping signals is conducted by calculating spatiotemporal correlation functions and identifying the associated decay length (L_0) [13]. Spearman's correlation index is applied within a square box extracted from the 2D-mapped tissue (Fig.1):

$$R(\vec{x},\vec{r}) = \frac{\langle (Y_A - \langle Y_A\rangle_t)(Y_B - \langle Y_B\rangle_t)\rangle_t}{\sigma_A \sigma_B} \tag{2}$$

where Y is a generic notation for ranks of voltage value at time t at positions $\vec{x}$ (Y_A) and $\vec{x}+\vec{r}$ (Y_B), and $\langle\cdot\rangle_t$ stands for time average computed over four depolarization fronts and respective repolarization backs. Finally, the characteristic length was extracted by evaluating a linear fitting of the exponential function $R(\vec{r}) = \exp\left(\frac{||\vec{r}||}{L_0}\right)$, in which $R(\vec{r})$ is the global correlation function composed by averaged correlation indices (Eq.2) over pixels separated by a variable distance $d \in [r, r+dr]$ [13].

We generalize previous contributions by introducing the normalized decay length (L_0^{MAX}) as a new metric to further improve the characterization of multiple transitions occurring during fast pacing regimes, defined as:

$$L_0^* = \frac{L_0^{MAX} - \langle L_0\rangle}{\langle L_0\rangle} \tag{3}$$

Here, $\langle L_0\rangle$ stands for the averaged decay length over four calculated beats at each PCL; L_0^{MAX} is the maximum value among them.

3. Results

We show how characteristic spatial length, further supported by spatial alternans maps and conduction velocity restitution curves, emphasize transmural heterogeneities in that one case of study of pathological human ventricle and it can represent a predictive index of arrhythmias onset.

3.1. Conduction velocity

Figure 3 displays averaged CV restitution curves high-

lighting distinct dynamics between epicardial and endocardial surfaces. Expected higher CV and steeper slopes are obtained on the endocardium layer combined with the presence of strong non-linearities, a signature of alternans development, at low PCL. These fluctuations are further associated with the onset of complex alternans patterns, as illustrated below.

Our measurements align with the literature, indicating differences up to 35 cm/s in averaged CVs between epicardium and endocardium planar excitation waves.

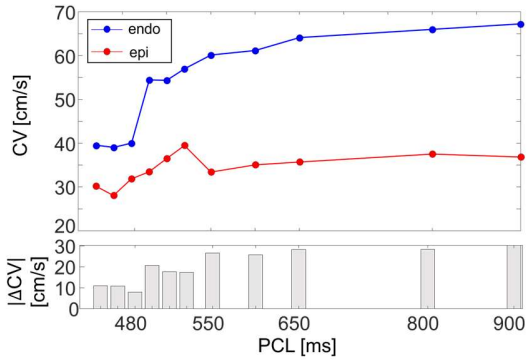

Figure 2. Conduction velocity [cm/s] restitution curves for human endocardium (blue) and epicardium (red), respectively. Mean values over four beats are shown. On the bottom, bar plot representing the absolute value of the difference, ΔCV, between ENDO-EPI mean CV values.

3.2. Alternans map

Spatial area alternans maps for selected pacing cycle lengths (PCL) are shown in Figure 2. The APD patterns were computed for both ENDO and EPI surfaces using Eq.1. The results (compared with restitution curves-not shown for the sake of space) show transition from non-alternating phases, SCA and SDA as PCL reduces. However, clear differences appear between ENDO and EPI with more pronounced discordant alternans observed on the endocardium as known from animal experiments [9].

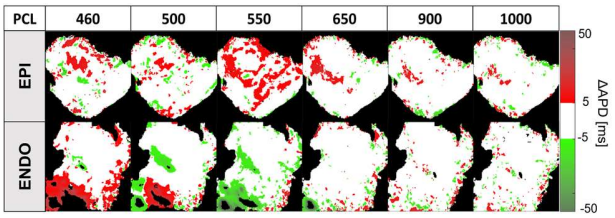

Figure 3. Spatial alternans maps for epicardium (EPI) and endocardium (ENDO) human ventricle at physiological temperature, organized row-wise. A red-green-white color scale is used to identify alternating pixels, according to Eq.1. Black pixels are out-of-mask pixels.

3.3. Spatiotemporal correlation analysis

Figure 4.A displays $\langle L_0 \rangle$ values computed during pacing-down restitution protocols on the endocardium (blue) and epicardium (red), respectively. Characteristic lengths show significant variations between tissues (with a $\Delta\langle L_0 \rangle$ ranging from 8 to 60 cm) as PCL varies from high (1000 ms) to low (420 ms) values.

It is noteworthy that lower correlation values are associated with a higher risk of arrhythmia onset. In fact, as previously observed in canine hearts [13], the correlation length reduces to ~1.7 cm, showing episodes of ventricular tachycardia immediately after, for which $\langle L_0 \rangle$ is ~1 cm (Fig.5).

Figure 4.B illustrates a comparison of the normalized correlation length (Eq.3), better emphasizing a transition zone during which the whole ventricle behaves synchronously (improving the known obtained from mean APD in canine hearts [9]). This novel feature, shown for the first time, is achieved during the PCL range of 700-600 ms and is characterized by a minimum difference, ΔL_0^*, implying a low intramural dispersion of the excitation wave. On the other hand, both at regular pacing, e.g., ~1000 ms, and at very fast ones, e.g., <500 ms, significant differences appear, thus implying a high degree of intramural dispersion within the ventricular wall. In particular, for PCL<500 ms, alternans onset induces oscillations of the intramural dispersion, critical features for wave breaks and spiral breakup.

Such an analysis opens toward the applicability of spatiotemporal correlation indices in extracting relevant characteristics for predicting arrhythmias.

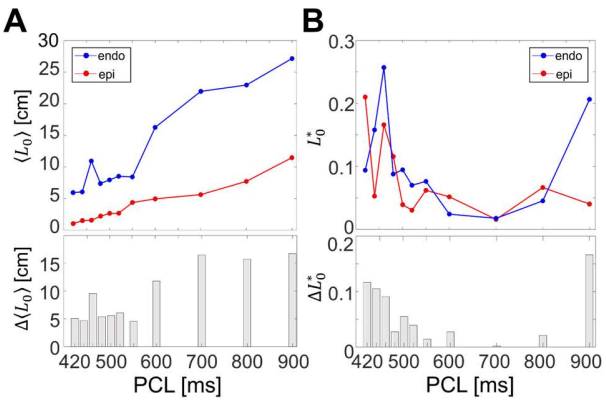

Figure 4. Comparison of (A) averaged characteristic spatial length, $\langle L_0 \rangle$, and (B) normalized characteristic length L_0^* (Eq.3), between human endocardial (blue) and epicardial (red) surfaces at physiological temperature (37°C) for different pacing cycle lengths. The bottom panel shows a bar plot indicating the endo-epi differences $\Delta\langle L_0 \rangle$ and ΔL_0^*, respectively.

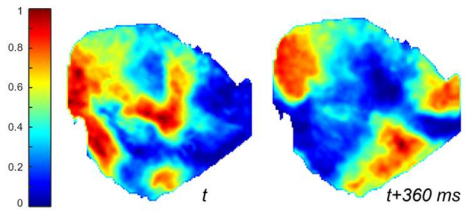

Figure 5. Representative example of epicardial ventricular tachycardia. Surface spiral waves frames at 360 ms on the whole epicardium. The averaged characteristic spatial length value reduces to $\langle L_0 \rangle \sim 1$ cm.

4. Discussion

The present contribution discusses a comprehensive spatiotemporal analysis of the endocardium and epicardium electrical dynamics of one pathological human heart. The results confirm what is in the literature regarding APD and CV differences between tissues, generalizing them in terms of spatial correlation length which can be interpreted as the total length of the excitation wave to physiologically synchronize the tissue restoring the resting state. As a result, differences, reduction, and oscillation of these values during paced excitations provide novel evidence of the transmural dispersion of repolarization. The latter can provide valuable insights into various arrhythmic onset mechanisms as it is related to the genesis of T-wave alternans.

Overall, characteristic spatial length potential applications in evaluating the effectiveness of different therapies, make it a promising pathway for improving the diagnosis and treatment of heart disease.

However, the differences in endo-epi dynamics could be a lot to do with scars distribution, highly variable from one heart to the next, and so an accurate study on the optical ultrastructure [14] could be associated to the proposed analyses for a more accurate comprehension of the underlying mechanisms.

Further studies will focus on contrasting voltage and calcium signal analyses [15] between synchronous endocardial and epicardial measurements. We are currently extending this study to incorporate temperature-dependent effects known to greatly influence the electro-physiological properties of the cardiac tissue [16, 17].

Acknowledgments

Authors acknowledge the support of the Italian National Group for Mathematical Physics (GNFM-INdAM).

References

[1] C S Kuo et al. “Characteristics and possible mechanism of ventricular arrhythmia dependent on the dispersion of action potential durations.,” Circ., vol. 67, no. 6 I, pp. 1356–1367, 1983.

[2] N T Srinivasan et al. “Dynamic spatial dispersion of repolarization is present in regions critical for ischemic ventricular tachycardia ablation,” Heart Rhythm O2, vol. 2, no. 3, pp. 280–289, Jun. 2021.

[3] R L Verrier et al. “Microvolt T-wave alternans: physiological basis, methods of measurement, and clinical utility—consensus guideline by international society for holter and noninvasive electrocardiology,” J Am Coll Cardiol, vol. 58, no. 13, pp. 1309–1324, Sep. 2011.

[4] J N Edwards et al. “Cardiac alternans and intracellular calcium cycling,” Clin Exp Pharmacol, vol. 41, no. 7, pp. 524–532, 2014.

[5] L. D. Wilson et al. “Heart failure enhances susceptibility to arrhythmogenic cardiac alternans,” Heart Rhythm, vol. 6, no. 2, pp. 251–259, 2009.

[6] I Uzelac et al. “Simultaneous quantification of spatially discordant alternans in voltage and intracellular calcium in langendorff-perfused rabbit hearts and inconsistencies with models of cardiac action potentials and ca transients,” Front Physiol, vol. 8, 2017.

[7] C Huang et al. “Stability of spatially discordant repolarization alternans in cardiac tissue,” Chaos, vol. 30, no. 12, p. 123141, Dec. 2020.

[8] A V Glukhov et. al “Translational research transmural dispersion of repolarization in failing and nonfailing human ventricle,” Circ, vol. 106(5), no. 397, pp. 981-91, 2010.

[9] A Gizzi, et al. “Effects of pacing site and stimulation history on alternans dynamics and the development of complex spatiotemporal patterns in cardiac tissue,” Front Physiol, vol. 4, 2013.

[10] S Kääb et. al, “Diversity of ion channel expression in health and disease,” EHJ, vol. 3, no. suppl_K, pp. K31–K40, Sep. 2001.

[11] I Uzelac et al. “Methodology for cross-talk elimination in simultaneous voltage and calcium optical mapping measurements with semasbestic wavelengths,” Front Physiol, vol. 13, 2022.

[12] A Savitzky et al. “smoothing and differentiation of data by simplified least squares procedures,” Anal Chem, vol. 36, no. 8, pp. 1627–1639, Jul. 1964.

[13] A Loppini et al. “Spatiotemporal correlation uncovers characteristic lengths in cardiac tissue,” Phys Rev E, vol. 100, 2020.

[14] A Loppini, et al. “Optical ultrastructure of large mammalian hearts recovers discordant alternans by in silico data assimilation,” Ftnep, vol. 2, 2022.

[15] Y Shiferaw et al. “Turing instability mediated by voltage and calcium diffusion in paced cardiac cells,” PNAS, vol. 103, no. 15, pp. 5670–5675, 2006.

[16] S Filippi, et al. “Mechanistic insights into hypothermic ventricular fibrillation: the role of temperature and tissue size,” EP, vol. 16, no. 3, pp. 424–434, Jan. 2014.

[17] A Loppini, et al. “Thermal effects on cardiac alternans onset and development: A spatiotemporal correlation analysis,” Phys Rev E, vol. 103, no. 4, p. L040201, Apr. 2021.

Address for correspondence:
Anna Crispino
Via Álvaro del Portillo, 21, Rome, Italy
anna.crispino@unicampus.it